Nonlinear Dynamics and Systems Theory, **24** (6) (2024) 582–593

Inducing Chaos through Timescales in a Three-Species Food Chain Model

Khadidja Daas * and Nasreddine Hamri

Laboratory of Mathematics and Their Interactions,
Departement of Mathematics, Boussouf Abdelhafid University Center,
Mila, Algeria

Received: April 1, 2024; Revised: November 2, 2024

Abstract: Over time, considerable attention has been devoted to understanding the complex dynamics of simplified ecosystems containing three trophic levels, revealing that complex behaviors can arise from a simple hierarchy between prey, predator, and top predator. In this study, the extension of a three-species food chain model with a Crowley-Martin-type functional response was examined by introducing discrete timescales to study its impact on system dynamics at various trophic levels. Changes in species abundance were analyzed across three different timescales: slow, fast, and intermediate. The presence of a homoclinic orbit in the subsystem (prey-predator) suggests the existence of period-doubling cascades that eventually lead to chaos in the entire system (prey-predator-top-predator). This study underscores the importance of ecological modeling and trophic interactions in understanding the diverse and intricate dynamics of ecosystems, thus highlighting the significance of research in this domain.

Keywords: *three-level trophic systems; time scales; chaos.*

Mathematics Subject Classification (2010): 37D45, 34C15, 37C75, 65L07, 70Kxx.

* Corresponding author: mailto:khadidja.daas@centre-univ-mila.dz

1 Introduction

A shift in focus towards understanding three-species systems resulted from the recognition that two-species systems are insufficient [7]. In seminal works, it has been demonstrated that models with three or more species can capture complex oscillatory dynamics within certain parameter ranges [4], [11], [8]. However, earlier studies of three-trophic level systems did not account for intraspecific rivalry at higher trophic levels, i.e., in top predators or predators. Thus, it was necessary to consider the potential impact of this rivalry on the system's dynamic properties. In a recent study, Peet et al. [1] added square terms to the equations for top predators and predators, thereby expanding Hastings-Powell's model. They demonstrated the importance of intraspecific rivalry in the evolution of chaotic trajectories by showing the coexistence of a chaotic attractor and a period-one cycle. They also showed how enhancing intraspecific competition among top predators can stabilize the system and pull it out of a chaotic state. Nevertheless, a critical component was absent from earlier research: the examination of various timescales at various trophic levels. Therefore, it is crucial that the modeling technique takes these various timelines into consideration. The system becomes singularly perturbed by adding several timescales, and geometric singular perturbation theory can be used to evaluate the system mathematically. This approach was first used by Rinaldi and Muratori [9] to examine slow-fast cycles in a three-species system on two timescales. They carried on more research and showed that species with slow, intermediate, and fast variables might cohabit oscillatory. In Hastings-Powell's model with several timescales, this was accomplished by employing singular perturbation techniques. Including several timescales can reveal far more complex dynamics like relaxation oscillations and canard cycles. These dynamics provide important new information for researching the occurrence of intricate chaotic oscillations. In our analysis, we used the method described in [6] to include three distinct timescales: slow, intermediate, and fast, and we divided the system into slow, intermediate, and fast subsystems. We investigated the three-species food chain model [10]. The results of each subsystem were then concatenated in order to look into the possibility of solitary slow-intermediate-fast cycles. Because of the intricacy of the model, numerical simulations were used to show that a homoclinic orbit exists inside a subsystem of the entire system. In the whole system, period-doubling cascades to chaos were seen simultaneously. The dynamics of the system changed either gradually or abruptly, depending on the degree of intraspecific rivalry among top predators. As a result, our research provides a possible framework for identifying and evaluating crucial changes that may cause an ecosystem to drastically change. This paper delves into the intricacies of a tri-trophic food web model, dissecting its dynamics and behaviors. Starting with the concept of a dimensionless model, the exploration seamlessly transitions to a meticulous reformulation of the three-species model using two dimensionless positive timescale parameters. In the subsequent section, the focus extends to a linear investigation and dynamic features. Equilibrium points are explored within the context of our study, contributing to a comprehensive understanding. Simultaneously, a detailed stability analysis is conducted, unraveling the nuanced intricacies. Moving through the paper, attention shifts to the dynamics of the subsystems, providing a granular perspective on their interplay and significantly contributing to the overall comprehension of the tri-trophic food web model. The exploration takes an intriguing turn in the final section, where chaos becomes the focal point. Introducing Lyapunov exponents as a lens to understand chaos, the paper concludes with an examination of the gradual entry into

chaos. Through this meticulously organized framework, the aim is to provide a holistic understanding of the tri-trophic food web model and its dynamic nuances.

2 A Tri-Trophic Food Web Model

2.1 Dimensionless model

The system under investigation in this work represents a mathematical model of a three-level food chain, which was transformed into a dimensionless model in [10]. The second order Holling pattern and the Crowley-Martin type functional response are combined in this food chain to form a hybrid type of organism.

$$\begin{cases} \dfrac{dX_1}{dT} = a_1 X_1 \left(1 - \dfrac{X_1}{K}\right) - \dfrac{cX_2X_3}{X_1 + D}, \\ \dfrac{dX_2}{dT} = -a_2 X_2 + \dfrac{c_1 X_1 X_3}{X_1 + D_1} - \dfrac{c_2 X_2 X_3}{1 + dX_2 + bX_3 + bdX_2X_3}, \\ \dfrac{dX_3}{dT} = -mX_3 + \dfrac{c_3 X_2 X_3}{1 + dX_2 + bX_3 + bdX_2X_3}, \end{cases} \tag{1}$$

where the population densities of the prey, predator, and top predator, respectively, as a function of time T are represented by the variables $X_1(T)$, $X_2(T)$, and $X_3(T)$.

As shown in Table 1, the model (1) is distinguished by the existence of 12 control parameters that regulate the behavior of the system.

Parameter	Description
a_1	The prey's intrinsic growth rate in the absence of predators
K	The prey's carrying capacity
D	Prey environmental protection
D_1	Predator environmental protection
c	The maximum rate of prey reduction per capita
c_1	Similar to c, the maximum rate of prey reduction per capita
c_2, c_3	Characteristics of the Crowley-Martin type functional response
b	Parameter assessing predator interference
a_2	Intermediate predator death rate X_2
m	Top predator death rate X_3

Table 1: Tri-trophic level food chain model parameters.

We simplified this model, ignoring dimensional considerations, to make the mathematical analysis easier. Table 2 contains dimensionless representations of the variables and parameters, where the first line represents the dimensionless variables, and the second line represents the corresponding environmental values.

t	x_1	x_2	x_3	c_4	c_5	c_6	c_7	c_8	c_9	c_{10}	c_{11}	c_{12}
a_1T	$\frac{X_1}{K}$	$\frac{cX_2}{a_1K}$	$\frac{cc_2X_3}{a_1^2dK}$	$\frac{D}{K}$	$\frac{a_2}{a_1}$	$\frac{c_1}{a_1}$	$\frac{D_1}{K}$	$\frac{a_1b}{c_2}$	$\frac{a_1^2bdK}{cc_2}$	$\frac{c}{a_1dK}$	$\frac{c}{a_1}$	$\frac{c_3}{a_1d}$

Table 2: Variables and parameters without dimensions.

As a result, we derived a dimensionless system characterized by nine parameters as detailed below:

$$\begin{cases} \dfrac{dx_1}{dt} = x_1 \left[(1 - x_1) - \dfrac{x_2}{x_1 + c_4} \right] = x_1 g_1(x_1, x_2), \\ \dfrac{dx_2}{dt} = x_2 \left[-c_5 + \dfrac{c_6 x_1}{x_1 + c_7} - \dfrac{x_3}{x_2 + (c_8 + c_9 x_2)\, x_3 + c_{10}} \right] = x_2 g_2(x_1, x_2, x_3), \\ \dfrac{dx_3}{dt} = x_3 \left[-c_{11} + \dfrac{c_{12} x_2}{x_2 + (c_8 + c_9 x_2)\, x_3 + c_{10}} \right] = x_3 g_3(x_2, x_3). \end{cases} \tag{2}$$

2.2 Reformulation of the three-species model

We employ two dimensionless positive timescale parameters, β_1 and β_2, to rescale the three-species model (2), with $0 < \beta_1, \beta_2 \ll 1$. The rescaling is done so that the growth rate of the predator is $O(\beta_1)$, and the growth rate of the top predator is $O(\beta_2)$. We reformulate the model (2) as follows after making this adjustment:

$$\begin{cases} \dfrac{dx_1}{dt} = x_1 \left[(1 - x_1) - \dfrac{x_2}{x_1 + c_4} \right] = x_1 g_1(x_1, x_2), \\ \dfrac{dx_2}{dt} = \beta_1 x_2 \left[-c_5 + \dfrac{c_6 x_1}{x_1 + c_7} - \dfrac{x_3}{x_2 + (c_8 + c_9 x_2)\, x_3 + c_{10}} \right] = \beta_1 x_2 g_2(x_1, x_2, x_3), \\ \dfrac{dx_3}{dt} = \beta_2 x_3 \left[-c_{11} + \dfrac{c_{12} x_2}{x_2 + (c_8 + c_9 x_2)\, x_3 + c_{10}} \right] = \beta_2 x_3 g_3(x_2, x_3). \end{cases} \tag{3}$$

The system's fast, intermediate, and slow variables, denoted by the values x_1, x_2, and x_3, respectively, reflect the dimensionless densities of prey, predators, and top predators. By putting the transformation $\tau_1 = \beta_1 t$ into (3), we may define the system and obtain the following results:

$$\beta_1 \frac{dx_1}{d\tau_1} = x_1 g_1(x_1, x_2), \frac{dx_2}{d\tau_1} = x_2 g_2(x_1, x_2, x_3), \beta_1 \frac{dx_3}{d\tau_1} = \beta_2 x_3 g_3(x_2, x_3), \tag{4}$$

and after additional changes $\tau_2 = \beta_2 t$, we obtain

$$\beta_2 \frac{dx_1}{d\tau_2} = x_1 g_1(x_1, x_2), \beta_2 \frac{dx_2}{d\tau_2} = \beta_1 x_2 g_2(x_1, x_2, x_3), \frac{dx_3}{d\tau_2} = x_3 g_3(x_2, x_3), \tag{5}$$

t, τ_1, and τ_2, the dimensionless time variables, represent the fast, intermediate, and slow time scales, respectively. We divide the system into subsystems and use geometric singular perturbation theory to study the dynamics of each one. For the systems (3), (4), and (5), a typical solution trajectory consists of segments corresponding to slow, intermediate, and fast processes. The total solution for the system is then obtained by concatenating the solutions of each subsystem (3). We initially investigate the impact of several time scales on the local dynamics of the system (3) before breaking it down into its component subsystems.

3 Linear Investigation and Dynamic Features

3.1 Equilibrium points

The number of non-negative equilibrium points in the system described by equation (3) can only be four. Table 3 summarizes the outcomes of the equilibrium point values and

associated conditions.

Equilibrium point	Values and conditions
P_0	Trivial equilibrium point: $(0,0,0)$
P_1	One-species equilibrium point: $(1,0,0)$
P_2	Two-species equilibrium point: $(\tilde{x_1},\tilde{x_2},0)$, where $\tilde{x_1}$ and $\tilde{x_2}$ are: $\tilde{x_1} = \frac{c_5 c_7}{c_6 - c_5}$ $\tilde{x_2} = (1-\tilde{x_1})(\tilde{x_1}+c_4)$ Existence condition: $0 < \frac{c_5 c_7}{c_6 - c_5} < 1$
P_3	Equilibrium point of coexistence of all three species (x_1^*, x_2^*, x_3^*) where: $x_2^* = (1-x_1^*)(x_1^*+c_4)$ $x_3^* = \frac{(c_{12}-c_{11})x_2^* - c_{10}c_{11}}{c_{11}(c_8+c_9 x_2^*)}$ Implicit equation for x_1^*: $-c_5 + \frac{c_6 x_1^*}{x_1^*+c_7} - \frac{x_3^*}{x_2^*+(c_8+c_9 x_2^*)x_3^*+c_{10}} = 0$ Existence conditions: $0 < x_1^* < 1$, $0 < \frac{c_{10}c_{11}}{c_{12}-c_{11}} < x_2^*$

Table 3: Equilibrium points and conditions.

3.2 Stability analysis

Every equilibrium point's Jacobian matrix was computed, and stability was examined using each matrix's characteristic polynomial. Table 4 summarizes the computation's findings.

Equilibrium Point	Jacobian Matrix	Eigenvalues
P_0	$\begin{pmatrix} 1 & 0 & 0 \\ 0 & -\beta_1 c_5 & 0 \\ 0 & 0 & -\beta_2 c_{11} \end{pmatrix}$	$e_1 = 1 > 0$, $e_2 = -\beta_1 c_5 < 0$, $e_3 = -\beta_2 c_{11} < 0$
P_1	$\begin{pmatrix} -1 & \frac{-1}{1+c_5} & 0 \\ 0 & \beta_1(\frac{c_6}{1+c_7} - c_5) & 0 \\ 0 & 0 & -\beta_2 c_{11} \end{pmatrix}$	$e_1 = -1$ $e_2 = \beta_1(\frac{c_6}{1+c_7} - c_5)$ $e_3 = -\beta_2 c_{11}$
P_2	$\begin{pmatrix} a_{11} & -a_{12} & 0 \\ \beta_1 a_{21} & \beta_1 a_{22} & -\beta_1 a_{23} \\ 0 & 0 & \beta_2 a_{33} \end{pmatrix}$	$e_0 = \beta_2 a_{33}$ $e_{1,2}(\beta_1) = \frac{a_{11}+\beta_1 a_{22}}{2} \pm$ $\frac{1}{2}\sqrt{(a_{11}-\beta_1 a_{22})^2 - 4a_{12}a_{21}}$

Table 4: Table of equilibrium points, Jacobian matrices, and eigenvalues.

Stability results and remarks:

- P_0 is always a saddle point.
- For P_1:

– If $c_5 < \frac{c_6}{1+c_7}$, then $\lambda_2 < 0$, and P_1 is a saddle point.
– If $c_5 > \frac{c_6}{1+c_7}$, then $\lambda_2 > 0$, and P_1 is stable.

- For P_2:

– The coefficients of the matrix J_{P_2} are

$$a_{11} = 1 - 2\tilde{x_1} - \frac{c_4(1-\tilde{x_1})}{\tilde{x_1}+c_4}, a_{12} = \frac{\tilde{x_1}}{\tilde{x_1}+c_4}, a_{21} = \frac{(1-\tilde{x_1})(\tilde{x_1}+c_4)c_6c_7}{(\tilde{x_1}+c_7)^2},$$

$$a_{22} = -c_5 + \frac{c_6\tilde{x_1}}{\tilde{x_1}+c_7}, a_{23} = \frac{(1-\tilde{x_1})^2(\tilde{x_1}+c_4)^2 + c_{10}(1-\tilde{x_1})(\tilde{x_1}+c_4)}{[(1-\tilde{x_1})(\tilde{x_1}+c_4)+c_{10}]^2},$$

$$a_{33} = -c_{11} + \frac{c_{12}(1-\tilde{x_1})^2(\tilde{x_1}+c_4)^2 + c_{10}c_{12}(1-\tilde{x_1})(\tilde{x_1}+c_4)}{[(1-\tilde{x_1})(\tilde{x_1}+c_4)+c_{10}]^2}$$

– We select c_5 as the bifurcation parameter in order to find the instability threshold for P_2. The Hopf bifurcation causes the equilibrium point P_2 to lose stability at $c_5 = \hat{c}_5$, where the real parts of the eigenvalues $e_{1,2} = 0$ are located. We select the parameters discussed in [10] and arrange them in Table 5, taking into account $\beta_1 = 1$, $\beta_2 = 1$.

Parameter	c_4	c_6	c_7	c_8	c_9	c_{10}	c_{11}	c_{12}
Value	0.25	0.8	0.25	0.01	0.1	0.28	0.06	0.25

Table 5: Parameter values.

We find that the real part of the eigenvalues $e_{1,2}$ equals zero at the value $\hat{c}_5 = 0,48$, from this, we reach the following results:

* If $c_5 < 0,48$, the equilibrium point P_2 is unstable.
* If $c_5 > 0,48$, the equilibrium point P_2 is stable.

To emphasize these results further, we provide an example, we select two values for c_5, and based on them, we calculate the equilibrium point P_2, and we analyze the stability in each case.

We present the results in Table 6.

c_5	Equilibrium point P_2	Jacobian matrix	Eigenvalues and stability
0.25	$(0.1136, 0.3223, 0)$	$\begin{pmatrix} -0.1136 & -0.3124 & 0 \\ -0.8254 & -0.9374 & -1.6603 \\ 0 & 0 & -0.3112 \end{pmatrix}$	0.1283, -1.1794, -0.3112 P_2 is unstable
0.5	(0.4167,0.3889,0)	$\begin{pmatrix} -0.4167 & -0.6250 & 0 \\ 0.300 & -1.2500 & -1.4950 \\ 0 & 0 & -0.3046 \end{pmatrix}$	$-0.8334 + 0.1181i$, $-0.8334 - 0.1181i$, -0.3046 P_2 is stable

Table 6: Stability study results for the dynamical system for two values of c_5.

- The interior equilibrium point $P_3 = (x_1^*, x_2^*, x_3^*)$:
We address the instability of the inner equilibrium point P_3 using a numerical example due to the intricacy of the equation involving x_1^*. We select the same set of parameter values with $c_5 = 0.25$, $\beta_1 = 1$, and $\beta_2 = 1$ as shown in Table 5. We use Liu's criteria to investigate the instability of P_3 via the Hopf bifurcation. Assume that the bifurcation parameter is c_{11}. We obtain that the matrix J_{P_3} has the characteristic equation as a function of c_{11}: $\lambda^3 + k_1(c_{11})\lambda^2 + k_2(c_{11})\lambda + k_3(c_{11}) = 0$, where $k_1(c_{11}) = 0.1412c_{11} - 0.0084187$; $k_2(c_{11}) = 7.8822 * 10^{-6}c_{11} - 0.025663$; $k_3(c_{11}) = 0.00023312 - 0.0038824c_{11}$. We consider $\Lambda(c_{11}) = k_1(c_{11})k_2(c_{11}) - k_3(c_{11})$, according to Liu's criteria [12], [3], P_3 becomes unstable through the Hopf bifurcation if there exists a critical value $\hat{c}_{11}$ such that $k_1(\hat{c}_{11}) > 0$, $k_3(\hat{c}_{11}) > 0$, $\Lambda(\hat{c}_{11}) = 0$, and $\left.\frac{d\Lambda}{dc_{11}}\right|_{c_{11}=\hat{c}_{11}} \neq 0$. After selecting the parameter values as previously indicated, we get $\hat{c}_{11} = 0.065964$. For $0 < c_{11} < 0.065964$, the coexistence equilibrium P_3 is stable; for $c_{11} > 0.065964$, it is unstable. We choose $\beta_1 = \beta_2 = 1$ and $c_{11} = 0.06$ as a specific case. Then $P_3 = (0.9240, 0.0893, 0.1412)$ is the only feasible coexistence equilibrium point. The Jacobian matrix evaluated at P_3, which is denoted as J_{P_3}, is given by

$$J_{P_3} = \begin{pmatrix} -0.9241 & -0.7871 & 0 \\ 0.3912 & -1.1659 & -2.6884 \\ 0 & 0.2551 & -0.2556 \end{pmatrix},$$

$\lambda^3 + k_1\lambda^2 + k_2\lambda + k_3 = 0$ is the characteristic equation of the matrix J_{P_3}, where $k_1 = 2.3455$, $k_2 = 2.6053$, and $k_3 = 0.9878$. Since $k_1 > 0$, $k_3 > 0$, and $k_1k_2 - k_3 = 5.1229 > 0$, we may conclude that P_3 is stable based on the Routh-Hurwitz criteria.

Choosing $c_{11} = 0.07$ and $\beta_1 = 0.7, \beta_2 = 0.49$ as another example yields unstable values $P_2 = (0.1136, 0.3223, 0)$ and $P_3 = (0.9046, 0.1101, 0.1482)$.

Figures 1, 2, and 3 will be used to illustrate this final example.

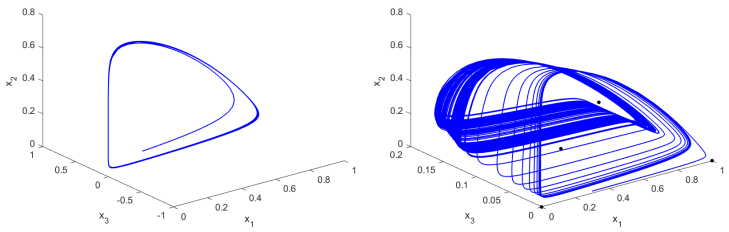

(a) (b)

Figure 1: Two trajectories converging to different periodic attractors, (a) Trajectory for $\beta_1 = 0.7$, $\beta_2 = 0.49$, initial point $=(0.2, 0.1, 0)$, (b) Trajectory for $\beta_1 = 0.7$, $\beta_2 = 0.49$, initial point $=(0.3, 0.1, 0.001)$.

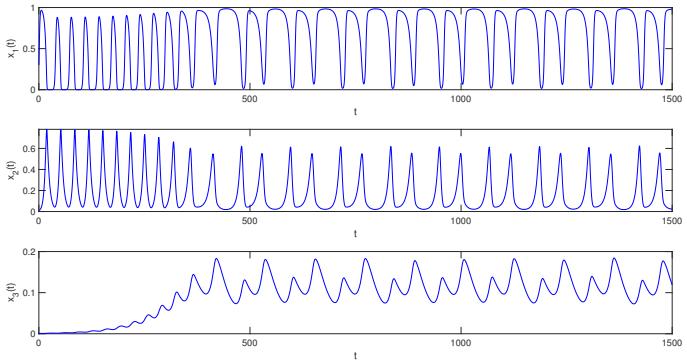

Figure 2: The frequencies of x_1, x_2, and x_3 as a function of time.

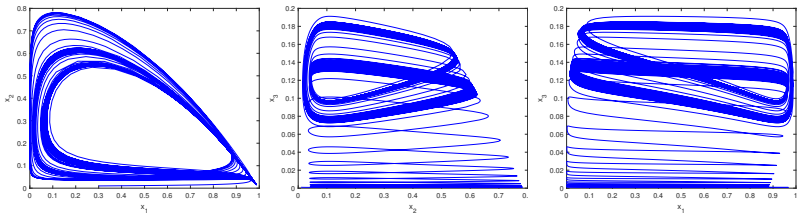

(a) (b) (c)

Figure 3: (a) Projection of the trajectory onto the x_1x_2 plane, (b) Projection of the trajectory onto the x_2x_3 plane, (c) Projection of the trajectory onto the x_1x_3 plane.

In the system, two stable limit cycles coexist: one around the equilibrium point P_2 in the x_1x_2 plane, and the other around P_3 in three-dimensional space, illustrating bistability. The trajectories are sensitive to initial conditions, suggesting the possibility of chaos.

4 Behavior of Subsystems

First, we present the model in the singular limit, that is, in the case when either $\beta_1 \to 0$ or $\beta_2 \to 0$, or both may occur. For $0 < \beta_1 < \beta_2 \ll 1$, the trajectory of the entire system (3) is a perturbed solution of subsystems. After time is divided into fast, intermediate, and slow timescales, we list the subsystems of the system (2) in Table 7. Concatenated slow-intermediate-fast flow, or the solutions of the aforementioned subsystems, make up the unique trajectory. A schematic example of a unique slow-intermediate-fast cycle is shown in Figure 4a, which consists of one slow flow segment (the thin black line), three segments of intermediate flows (the medium blue line), and two segments of fast flows (the thick red line). The critical manifold of the fast subsystem is the set of all equilibrium points as follows:

$$M^0 = \{(x_1, x_2, x_3) : x_1 = 0, x_2, x_3 > 0\}, \quad M^1 = \{(x_1, x_2, x_3) : g_1(x_1, x_2) = 0, x_3 > 0\},$$

Condition	Subsystem
$\beta_1 \to 0$ (Fast)	$\begin{cases} \frac{dx_1}{dt} = x_1\left[(1-x_1) - \frac{x_2}{x_1+c_4}\right] = x_1 g_1(x_1,x_2), \\ \frac{dx_2}{dt} = 0, \\ \frac{dx_3}{dt} = 0. \end{cases}$
$\beta_2 \to 0, \beta_1 > 0$ (Intermediate)	$\begin{cases} \frac{dx_1}{dt} = 0, \\ \frac{dx_2}{dt} = \beta_1 x_2\left[-c_5 + \frac{c_6 x_1}{x_1+c_7} - \frac{x_3}{x_2+(c_8+c_9x_2)\,x_3+c_{10}}\right] = \beta_1 x_2 g_2(x_1,x_2,x_3), \\ \frac{dx_3}{dt} = 0. \end{cases}$
$\beta_1, \beta_2 \to 0$ (Slow)	$\begin{cases} \frac{dx_1}{dt} = 0, \\ \frac{dx_2}{dt} = 0, \\ \frac{dx_3}{dt} = x_3\left[-c_{11} + \frac{c_{12}x_2}{x_2+(c_8+c_9x_2)\,x_3+c_{10}}\right] = x_3 g_3(x_2,x_3). \end{cases}$

Table 7: Description of subsystems in the model.

it expressly looks like this $M^1 = \{(x_1, x_2, x_3) : x_2 := \varphi(x_2) = (1 - x_2)(x_2 + c_4), x_2 > 0, x_3 > 0\}$. There is a fold in this surface, and we can find the fold curve by $\mathcal{C} = \{(x_1, x_2, x_3) : \varphi'(x_1) = 0, x_2 = \varphi(x_1), x_3 \geq 0\}$, implying $x_{1,max} = \frac{1-c_4}{2}$.

With the exception of the fold curve $\mathcal{C}$, where it loses its hyperbolicity, M^1 is hyperbolic everywhere. The non-trivial critical manifold $M^1 = 0$ is divided into typically hyperbolic attracting and repelling sub-manifolds by the fold curve $\mathcal{C}$ as follows: $M^1_a = \{(x_1, \varphi(x_1), x_3) : x_1 > x_{1,max}, x_3 \geq 0\}$ and $M^1_r = \{(x_1, \varphi(x_1), x_3) : x_1 < x_{1,max}, x_3 \geq 0\}$, respectively. The trivial critical manifold M^0 (x_2x_3-plane) and the manifold M^1 intersect at a curve that is described by $\mathcal{T}_1 = \{(0, c_4, x_3) : x_3 \geq 0\}$.

The transcritical bifurcation curve, $\mathcal{T}_1$, splits the plane into hyperbolic sub-manifolds that are typically repellent and attractive, respectively. Next, the manifold M_0's attracting and repelling sub-manifolds are $M^0_a = \{(0, x_2, x_3) : x_2 > \varphi(0), x_3 > 0\}$, and $M^0_r = \{(0, x_2, x_3) : x_2 < \varphi(0), x_3 > 0\}$, respectively.

For β_1, β_2, where $0 < \beta_1, \beta_2 \ll 1$, Fenichel's theorem [5] guarantees the existence of locally invariant perturbed sub-manifolds, the essential manifolds M^0 and M^1 have the sub-manidolds $M^0_{\beta_1,\beta_2}$ and $M^1_{\beta_1,\beta_2}$, respectively, with the exception of the non-hyperbolic curves $\mathcal{C}$ and $\mathcal{T}_1$. Additionally, the corresponding attracting M^1_{a,β_1,β_2} and repelling M^1_{r,β_1,β_2} sub-manifolds are perturbed by the attracting (M^1_a) and repelling (M^1_r) sub-manifolds of the critical manifold. Consequently, the perturbed sub-manifolds $M^0_{\beta_1,\beta_2}$ and $M^1_{\beta_1,\beta_2}$ dictate the dynamics of the entire system (3) for $\beta_1, \beta_2 \neq 0$ locally.

The intermediate subsystem is defined on the manifolds M^0 and M^1 with $x_3 =$ constant, therefore we analyze the intermediate system in the plane $x_3 = c'$, parallel to the x_1x_2-plane. Substituting $x_3 = c'$ in the expression of g_3, we obtain an explicit expression of the non-trivial nullcline of the intermediate subsystem as follows:

$$x_1 = \frac{c_5c_7(1 + c_9c')x_2 + (c_5c_7c_8 + c_7)c' + c_5c_7c_{10}}{(c_6 + c_9(c_6 - c_5)c' - c_5)x_2 + (c_6c_8 - c_5c_8 - 1)c' + c_{10}(c_6 - c_5)}. \tag{6}$$

The number of equilibrium points is related to the value c' and other background parameters.

For example, in Figure 4b, we represents that for $c' = 0.1$, the system has a unique unstable equilibrium surrounded by a stable limit cycle.

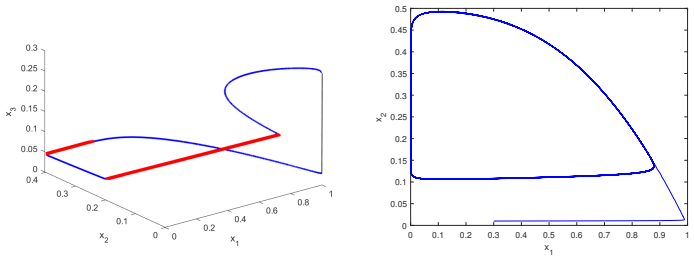

(a) (b)

Figure 4: The dynamics of the subsystems: (a) A schematic representation of the slow-intermediate-fast cycle for $\beta_1 = 0.005$ and $\beta_2 = 0.0035$, (b) The dynamics of the intermediate systems for $c = 0.1$, $\beta_1 = 0.1$ and $\beta_2 = 0$.

Understanding the dynamics generated by the intermediate subsystem of the complete system is particularly important for certain specific instances. The primary goal of this work is to examine many chaotic dynamics that the system (3) exhibits and to find out how the system's chaotic regimes may be impacted by the various timescales.

5 Dynamical Analysis of Chaos

5.1 Lyapunov exponents

We represented the Lyapunov exponents by assuming two values for β_1 and β_2 and obtained the following results.

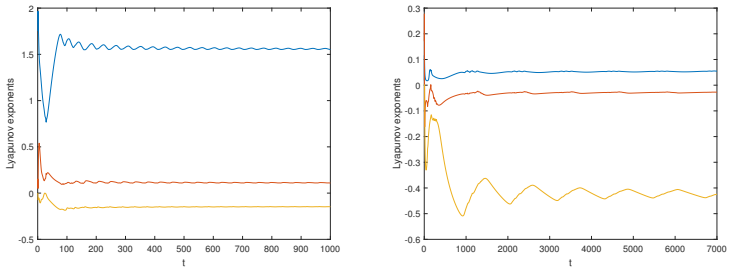

(a) (b)

Figure 5: (a) Lyapunov exponents for $\beta_1 = 1, \beta_2 = 1$, (b) Lyapunov exponents for $\beta_1 = 0.1, \beta_2 = 0.05$.

Comparison: The presence of this type of Lyapunov exponents in Figure 5a indicates greater complexity in the system's behavior, where there is local convergence in one direction with dispersion or chaos in others. This suggests a higher sensitivity of system (2) to initial conditions compared to the system after temporal segmentation (3), resulting in a more complex and chaotic behavior. The role of this study using temporal segmentation becomes evident, as it has made the system's behavior clearer.

5.2 Entering chaos gradually

We demonstrate how the timescales parameters affect the chaotic dynamics. Our simulations begin at $\beta_1 = \beta_2 = 1$ and are progressively decreased to determine the period-doubling cascade that leads to chaos. In Figure 6a, we note that the species live along a periodic orbit in the absence of multiple timescales. On the other hand, in Figure 6b, the 1-periodic orbit experiences a period-doubling bifurcation as β_1 and β_2 decrease, we achieve a 2-periodic orbit. In Figure 6c, we obtain a 4-periodic orbit. Thus, with consecutive period-doubling bifurcations, the system becomes chaotic from periodic (see Figure 6d).

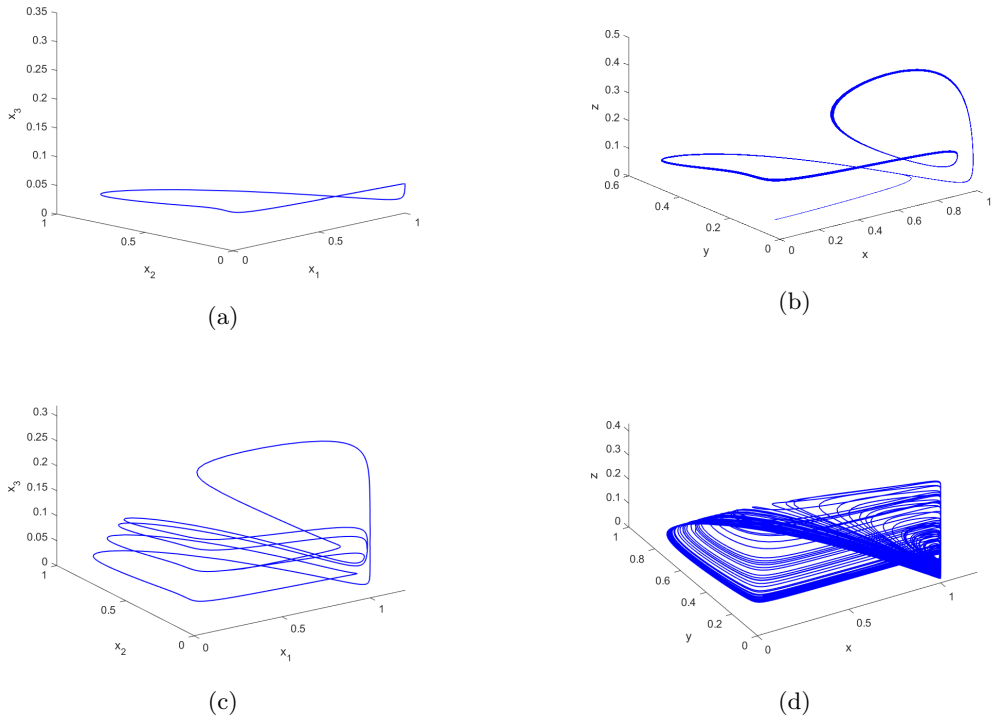

Figure 6: The periodic-doubling bifurcation with varying β_1 and β_2, (a) Period 1 for $\beta_1 = 1$ and $\beta_2 = 1$, (b) Period 2 for $\beta_1 = 0.25$ and $\beta_2 = 0.125$, (c) Period 4 for $\beta_1 = 0.2$ and $\beta_2 = 0.1$, (d) Chaos for $\beta_1 = 0.1$ and $\beta_2 = 0.05$.

6 Conclusion

The ecological interpretations of the results presented in this paper underscore the importance of understanding the environmental impacts of changes in key parameters of environmental models. As the reproduction rate of the first predator approaches zero, it reflects the environmental response of the food chain and predators. Reducing the reproduction rate leads to a decrease in the population of the first predator, indirectly affecting the higher predator, which relies on the first predator as a food source. It is worth noting

that the environmental effects of these changes are not limited to the individual level but also extend to the ecosystem level as a whole. Due to the complex interactions between living organisms and environmental factors, the ecosystem can transition into a state of chaos, where behavior becomes unpredictable and dynamics are unstable. Therefore, this research sheds light on the importance of analyzing the environmental impacts of changes in the key parameters of environmental models and their role in determining the stability and evolution of ecosystems in the long term.

In summary, this research makes a significant contribution to understanding the environmental impacts of changes in ecological systems and identifying factors that influence their stability. This helps in developing strategies for conserving biodiversity and ensuring environmental sustainability.

References

[1] A. Peet, P. Deutsch and E. Peacock-López. Complex dynamics in a three-level trophic system with intraspecies interaction. *Journal of Theoretical Biology* **232** (4) (2005) 491–503.

[2] B. Deng and G. Hines. Food chain chaos due to Shilnikov's orbit. *Chaos: An Interdisciplinary Journal of Nonlinear Science* **12** (3) (2002) 533–538.

[3] D. Sen, S. Ghorai and M. Banerjee. Complex dynamics of a three species prey-predator model with intraguild predation. *Ecological Complexity* **34** (2018) 9–22.

[4] M. Benkara and N. Hamri. Stability and Hopf bifurcation of generalized differential- algebraic biological economic system with the hybrid functional response and predator Harvesting. *Nonlinear Dynamics and Systems Theory* **23**(4) (2023) 398–409.

[5] N. Fenichel. Geometric singular perturbation theory for ordinary differential equations. *Journal of differential equations* **31** (1) (1979) 53–98.

[6] P. Chowdhury, M. Banerjee and S. Petrovskii. Coexistence of chaotic and non-chaotic attractors in a three-species slow–fast system. *Chaos, Solitons & Fractals* **167** (2023) 113015.

[7] P. Price, C. Bouton, P. Gross, B. McPheron, J. Thompson and A. Weis. Interactions among three trophic levels: influence of plants on interactions between insect herbivores and natural enemies. *Annual review of Ecology and Systematics* **11** (1) (1980) 41–65.

[8] R. Ouahabi and N. Hamri. *Systèmes dynamiques et chaos*. PhD thesis, Universitè Frères Mentouri-Constantine 1, 2018.

[9] S. Rinaldi and S. Muratori. Slow-fast limit cycles in predator-prey models. *Ecological Modelling* **61** (3-4) (1992) 287–308.

[10] U. R. Kumar and N. R Kamel. Dynamics of a three species food chain model with Crowley–Martin type functional response. *Chaos, solitons & fractals* **42** (3) (2009) 1337–1346.

[11] W. Laouira and N. Hamri. New Design of Stability Study for Linear and Nonlinear Feedback Control of Chaotic Systems. *Nonlinear Dynamics and Systems Theory* **22** (4) (2022) 414–423.

[12] W. Liu. Criterion of Hopf bifurcations without using eigenvalues. *Journal of Mathematical Analysis and Applications* **182** (1) (1994) 250–256.